Sensors and Actuators B 257 (2018) 37–47

Contents lists available at ScienceDirect

Sensors and Actuators B: Chemical

journal homepage: www.elsevier.com/locate/snb

Research Paper

# Non-labeled selective virus detection with novel SERS-active porous silver nanofilms fabricated by Electron Beam Physical Vapor Deposition

Nikolay N. Durmanov[a,*], Rustam R. Guliev[a], Arkady V. Eremenko[a], Irina A. Boginskaya[b], Ilya A. Ryzhikov[b,c], Ekaterina A. Trifonova[d], Egor V. Putlyaev[d], Aleksei N. Mukhin[e], Sergey L. Kalnov[e], Marina V. Balandina[e], Artem P. Tkachuk[e], Vladimir A. Gushchin[e], Andrey K. Sarychev[b], Andrey N. Lagarkov[b], Ilya A. Rodionov[c,f], Aidar R. Gabidullin[c,f], Ilya N. Kurochkin[a,d]

[a] Emanuel Institute of Biochemical Physics of Russian Academy of Sciences, Kosygina 4, 119991, Moscow, Russia
[b] Institute for Theoretical and Applied Clectromagnetics Russian Academy of Sciences, Ijorskaya 13, 125412, Moscow, Russia
[c] Bauman Moscow State Technical University, 2-ya Baumanskaya 5/1, 105005, Moscow, Russia
[d] Lomonosov Moscow State University, Leninskie gory 1, 119991, Moscow, Russia
[e] Gamalei Science Research Center of Epidemiology and Microbiology, Russian Ministry of Health, Gamalei 16-18, 123098, Moscow, Russia
[f] Dukhov Research Institute of Automatics, Sushchevskaya 22, 127055, Moscow, Russia

ARTICLE INFO

*Article history:*
Received 30 March 2017
Received in revised form
30 September 2017
Accepted 3 October 2017
Available online 5 October 2017

*Keywords:*
SERS
Raman spectroscopy
Viruses
Biosensing
Physical vapor deposition

ABSTRACT

Virus detection is often performed using antibody-based and polymerase chain reaction-based techniques. Such methods have major deficiencies, caused by time-consuming and labor-intensive incubation and purification steps. In this contribution, a novel SERS substrate for qualitative virus detection was developed and described. The substrate is composed of a thin silver film with folded surface structure containing pore-like nanoscale cavities and indentations, deposited on mica substrate by electron beam physical vapor deposition method. Pore-like structures are semi-regularly arrayed, with a rough surface in between, allowing for SERS activity, and their size and periodicity can be manipulated in the manufacturing process. It was speculated that viral particles could be trapped in these structures and would generate easily detectable enhanced Raman signals. The SERS substrate was tested against detection of four virus species – rabbit myxomatosis virus, canine distemper virus, tobacco mosaic virus and potato virus X. Specific spectra were obtained and analyzed for each virus. Data analysis demonstrated successful differentiation between tested species. The reported results demonstrate that novel SERS substrate is suitable for detection and identification of viral particles.

© 2017 Published by Elsevier B.V.

## 1. Introduction

The emergence of various new biological threats across the globe caused the worldwide increase in attention to matters of detection and identification of dangerous pathogens. Major efforts are directed towards the development of potential rapid and accurate techniques, that would allow detection and identification of pathogens at early stages in disease monitoring systems [1,2]. While there are a number of methods already available for detection of viruses, such as antibody-based techniques [3] or approaches based on polymerase chain reaction (PCR) [4], they remain largely impractical for on-site rapid detection, mostly due to complexity of preliminary steps, required for isolation of target species, and limitations imposed by required specificity of antibodies or primers [5].

There is a need for simpler ways to detect and identify viral particles. There are, however, certain challenges involved, associated with necessary purification steps, variation in particle shape and dimensions, need for high sensitivity and establishment of identification databases, as well as many other issues [6,7]. While it is possible to investigate biomolecules using, for instance, resonating mechanical cantilevers [8], evanescent wave biosensors [9], atomic force microscopy [10] and various other techniques, most of them have weak points, are time-consuming, require a label-

*Abbreviations:* EBPVD, electron beam physical vapor deposition; MYXV, Myxoma virus; CDV, canine distemper virus; TMV, tobacco Mosaic virus; PVX, potato virus X.

* Corresponding author.
*E-mail addresses:* durmanstain@gmail.com, durmanstein@gmail.com (N.N. Durmanov).

https://doi.org/10.1016/j.snb.2017.10.022
0925-4005/© 2017 Published by Elsevier B.V.

ing method in order to bind particular target molecule or particle [11,12]. The ability to detect new targets is often limited, depending on specific probes, labels and preexisting entry in the database. Meanwhile, label-free detection becomes more and more necessary, as the majority of serious viral outbreaks for the past several decades have been caused by newly emerging viral species [13,14].

Recently, there has been an increasing interest in the development of nanoplasmonic substrates with a controlled surface structure for spectroscopic applications [15,16]. The progress on the detection of microorganisms has demonstrated a significant potential for future application of the effect of surface-enhanced Raman scattering (SERS) for rapid detection of pathogens, including viruses [17–19]. The method does not require extensive sample preparation steps, which enables detection of fragile and sensitive objects. While viruses are usually found in water and air in relatively low concentrations, SERS was also shown to have high enough sensitivity to detect trace amounts of biomolecules and, under special circumstances, even capable of single-molecule detection [20]. Theoretically, SERS can be even applied to categorize unknown viruses by their spectra, based on spectral similarities between species of the same group [21].

To produce the surface enhancement effect, the surface must be composed of a particular metal (i.e. Au, Ag, Cu) and have certain nanoscale features and topologies, often generally described as "roughness" [22–24]. The roughened surface can be made of deposited nanoparticles or as a structured array. Overhaul, any rough silver or gold surface can demonstrate signal enhancement, though to a vastly different extent, depending on specific surficial properties [25,26]. In SERS studies of biological targets, there is a major challenge of crafting not just a SERS-substrate with strong EF, but a biointerface that can tightly interact with the attached biomolecules [27]. To achieve sufficient levels of enhancement, apart from dealing with plasmonic properties of the SERS substrate, one must address the effective distance between the tailored surface and the target molecules or particles. In many of the published works related to SERS studies of viruses, it is assumed, that to achieve sufficient enhancement indentations and nanoscale cavities are necessary, with characteristic sizes equal to or bigger than the sizes of viral particles [28]. It is generally speculated, that particles are trapped in such pits, and this increases the area of interaction between a virus and a SERS surface, which in turn leads to a higher amount of viral material generating SERS signals.

Many different types of SERS substrates have been described over the years; however, each type has its advantages and disadvantages that are tightly correlated with the method of fabrication. In general, fabrication techniques can be sorted into several categories, including top-down and bottom-up types [27]. Top-down techniques are usually more expensive and slow, but also more precise and controllable, with the exception of the oxidation-reduction cycling of a metal electrode surface, which was the first type of substrate used and is still in use for fundamental studies [29]. In this case, precise control of the surface morphology is hard to obtain, and it leads to low SERS reproducibility [30]. In contrast, electron beam lithography and other lithographic techniques can achieve accurate, controllable, and reproducible arrays of nanostructures, however, each structural unit has to be fabricated one at a time in a serial manner [30,31], which means only a relatively small sensing area (typically, less than 100 μm across) can be fabricated in a reasonable time and at a reasonable cost. Metal colloids are also popular as SERS substrates due to a simple fabrication process, but they often lack sensitivity and reproducibility [26,32]. Bottom-up techniques can be much easier to apply, cheaper and faster, but suffer from lower reproducibility. One such example is the immobilization of plasmonic nanoparticles on a solid base: synthesizing and depositing nanoparticles is a relatively simple task, but controlling the uniform nanoparticle dispersion over a larger area is in fact very challenging. There are several successful examples, such as using dielectric substrates with immobilized plasmonic nanoparticles [33,34], but they are also subjected to major limitations on possible types of surface morphology. However, for large scale application, bottom-up methods appear to have great potential due to lower cost and relative ease of fabrication.

In the present study, a novel SERS substrate, in the form of a silver nanofilm, was manufactured through physical vapor deposition (PVD), featuring a complex semi-regular roughened surface structure with pore-like indentations and folds. It bears certain key similarities to arrays of nanoscale cavities, which have been demonstrated to possess high potential for SERS detection of viruses [28,35]. PVD has been traditionally used for the semiconductor and optical coating to uniformly deposit smooth metal films over a large area. In SERS application PVD has also been heavily employed to produce SERS-active nanostructured metal surfaces. Most of the time, such substrates have been presented by metal "island" nanostructures or, alternatively, thin metal films deposited onto a pre-patterned template [36,37]. One of the more popular applications is the oblique angle PVD method, often used to produce the arrays of nanorods [38]. When it comes to porous surfaces, the majority of researchers turn to other techniques. In this contribution, it is shown, that direct PVD methods are also suitable to manufacture such SERS-active surfaces.

The electron beam evaporation technique (EBPVD) was used in particular, due to its fast deposition rate. Usually, it is used for coating surfaces with smooth layers of metals. To manufacture a SERS-substrate, the general idea is to intentionally "sabotage" the coating process, making a disrupted metal film with a rough surface. The precise nanostructure of the fabricated metal films is controlled by the microstructure of the substrate, temperature, evaporation/deposition speed, as well as other process characteristics [39,40]. Adjusting these variables, it is possible to obtain metal films with reproducible and controllable surface morphology. Some of these dependencies have been determined in preliminary experiments. Certain combinations can be used to manufacture thin silver nanofilms with pore-like semi-regular structures, where the "pore" sizes and the surface roughness can be adjusted in a controlled manner.

The application of such controlled nanocavities was tested against accommodation and collecting SERS spectra of large viral particles with diameters in the range of 100–300 nm. It is anticipated, that this new technique proves to be an easy, cost-effective and highly reproducible method to make tailored SERS-active surfaces, capable of reliable discrimination between different species of viruses.

Four species were selected to demonstrate practical application of the novel SERS substrate, two enveloped viruses, known to cause diseases in mammals – Myxoma virus (MYXV) [41], a member of Poxviridae, and Canine Distemper virus (CDV) [42], from Paramixoviridae, and two non-enveloped plant disease viruses – Tobacco Mosaic virus (TMV) [43], from Virgaviridae, and Potato virus X (PVX) [44] from Alphaflexiviridae. The novel SERS substrate was tested on its capabilities in acquiring spectra of viral particles with entirely different size, morphology, structural composition, physicochemical properties. Various methods of data analysis were used to attempt identification of viruses based on their spectra.

## 2. Materials and methods

### 2.1. The fabrication of nanoscale silver films with developed surface morphology

Thin silver nanofilms were deposited on mica substrate (approximately 100 μm thick) by EBPVD method, using the Evovac

(Angstrom Engineering Inc., Canada) tool. The base vacuum was set to $3 \times 10^{-8}$ Torr. The voltage of the power feed for the evaporator ranged from 9 to 11 kV, with the distance between mica substrate and the vapor source 300 mm. Mica plates were prepared by washing with isopropyl alcohol and then split with a specialized razor and immediately loaded into the vacuum chamber. Silver powder (99,999% purity) was placed into molybdenum crucible and evaporated under focused electron beam. The speed of evaporation was manipulated by altering the current at electron beam evaporator power source, monitored by quartz control sensor (Inficon), and was varied in the range of 1–4 Å$s^{-1}$. The average thickness of all fabricated silver nanofilms was set to reach 150 nm as measured with the stylus profilometer (KLA-Tencor, USA), and the temperature of substrate holder during deposition was set to 400 °C. Such parameters allowed manufacturing of silver films with strongly developed surface morphology.

### 2.2. Characterization of the surface structure

The surface morphology was characterized by Atomic Force Microscopy (AFM) (Solver, NT-MDT, Russia), in the semicontinuous mode in repulsion regime with HA – NC cantilever with resonance frequency 149 kHz ± 10%, force constant 3.5 N/m, tip radius less than 10 nm, coated with Au. The cantilever was made of polycrystalline silicon, the shape of the probe octahedral at the base and conical for the furthermost 200 nm, chosen for a precise preservation of the resonance frequency during measurements and high stability. The full height of the probe was 10 μm. Each line was scanned by two passes – the first for Mag signal, proportional to the height changes, the second for measuring phase changes in comparison to the base signal, sensitive to minor terrain irregularities. The scan resolution was $256 \times 256$ and $512 \times 512$ pixels, scanning speed 1 Hz, the probe oscillation amplitude 0,2 V. The residual charge was removed from the nanofilms before the study for better resolution.

In conjuncture with the AFM, the SERS substrates were studied with Scanning Electron Microscopy (SEM) (Zeiss, Germany). In-Lense SE secondary electron detector was used in low voltage mode for low sample conductivity, the beam acceleration voltage was EHT 5 kV, the pressure in the chamber $10^{-6}$ mbar. The noise suppression was achieved by pixel averaging of the images during scanning by 20 pixels.

The focal distance was 5 mm, the beam current 134 pA. The resulting resolution was <1 nm.

The state of silver on the surface was determined by X-ray Photoelectron Spectroscopy (Axis Ultra DLD, Kratos Analytical, Japan) with transmission energy of 160 eV for the panoramic measurement, and 40 eV for high-resolution measurement.

The thickness of the films and the surface roughness were measured with stylus profilometer using the Durasharp stylus with curvature radius 40 nm, the lateral resolution 25 nm, the z-axis resolution 0.4 nm, with low force measurements 0.05 mg for sample preservation. The scanning speed was 50 μm/s, with 500 nm long profilograms. Rq and the kurtosis coefficient were determined according to standard formulas [45]:

$$\mathrm{Rq} = \sqrt{1/n \sum_{i=1}^{n} y^2},$$

$$\mathrm{Rku} = \frac{1}{nR_q^3} \sum_{i=1}^{n} y^4,$$

where $y$ is the terrain height.

To determine thickness, the nanofilms were cut with a scriber. The depth of the scratch was then determined with profilometer and represents the thickness of the silver film.

The pore sizes were derived from AFM $5 \times 5$ μm images with Gwyddion software. The standard grain analysis feature was used to determine the pore area by applying the inverted mask at the edges. Average depth and width were evaluated with profilograms.

### 2.3. Preparation of viruses

MYXV vaccine strain IS-14 was propagated on Vero (African green monkey kidney) cells in Dulbecco's modified Eagle's medium (DMEM) supplemented with 10% fetal bovine serum in a 5% CO2 atmosphere at 37 °C. The cells were infected with myxoma virus (strain IS-14) at a multiplicity of infection of 0.1, cultured for 5–6 days. At maximum growth, the culture medium was replaced with serum-free DMEM. Then cells were harvested by scraping the cells into the media and recovering them by low-speed centrifugation. The cells were broken by freeze-thaw, and viral particles were concentrated and purified using a combination of modified standard procedures for MYXV and vaccinia virus, by ultracentrifugation through sucrose density gradients [46].

CDV "Ondeersteport" strain was propagated on Vero cells the same way and purified from serum-free DMEM with modified protocol. The virus was concentrated by ammonium sulfate precipitation [47], resuspended and purified by density gradient centrifugation [48], then dialyzed against 10 mM tris-HCl (pH 8.0).

Characterization of purified viruses was performed with a combination of methods. Real-time PCR [49] was used for MYXV and ELISA for CDV. Virus samples were subjected to absorption spectroscopy to determine nucleic acid and protein concentration (Nanodrop 2000, Thermo, USA), and Transmission Electron Microscopy (TEM) (JEOL JEM-1011, JEOL, Japan), performed at 80 kV, results recorded with a Gatan Erlangshen ES500W digital camera, and processed with a GATAN DIGITAL MICROGRAPH software (Gatan, Pleasanton, CA, USA). To calculate sizes, micrographs were analyzed by image manipulation software IMAGEJ (National Institutes of Health, Bethesda, MD, USA).

TMV strain U1 was isolated from systemically infected Nicotiana tabacum L. cv. Samsun plants as described previously [50]. The virus was extracted from plant material, concentrated with PEG precipitation and purified by two-stage differential centrifugation with sucrose cushion. Likewise, the Russian strain of PVX was isolated from infected plants (Datura stramonium L.) as described previously [51]. Both TMV and PVX were characterized by the same set of methods, including TEM, Nanoparticle Tracking Analysis, RNA electrophoresis.

The purified viruses were stored either at −80 °C (MYXV and CDV) or at +4 °C (TMV and PVX). Prior to SERS measurement viruses were transferred to 10 mM tris-HCl solution (pH 8.0). For MYXV and CDV, control extracts were prepared from mock-infected cells and comparable volumes of material processed identically. Controls for TMV and PVX were made from non-infected plant extracts of appropriate volume, subjected to the same procedures. As a common control solution, a 10 mM tris-HCl (pH 8.0) solution was used. Additionally, high purity glucose was dissolved in control solution (0.1 g/l) as a test sample for demonstrating general SERS activity of the novel substrates.

### 2.4. SERS measurement experimental setup

The spectra measurements were performed on Alpha300 R Raman spectroscopy confocal microscope (WiTec, Germany), with 785 nm diode laser (XTRA high-power 785 nm, Toptica Photonics, Germany) and CCD detector (UHTS300, Andor, Ireland). Laser power on SERS substrate surface was set at the total of 18 mW,

focused through a 50× air objective lens, with illuminated spot being about 900 nm in diameter. Scattered light was collected by the same 50× lens and transferred via optical fiber to the CCD detector. A grating of 600 lines/mm was used to disperse scattered light. Integration time varied from sample to sample, and was set to remain less than 120 s, with optimal time being chosen for each sample to acquire maximum intensity of the spectrum, but without overflow.

Measurement process started with sample deposition on the SERS substrate. All samples were diluted to the concentration of $1 \times 10^{11}$ particles per ml, thoroughly mixed, and then 3 μl of the resulting solution was carefully placed with laboratory pipette on the surface of the SERS substrate, without touching it. The sample was dried at room temperature for 20 min. Spectra were accumulated at equal intervals of 40 μm between each measurement position. Before each accumulation, laser power was lowered to 2 mW; then the optical system was focused along the z-axis, achieving a maximum intensity of the scattered light at 60–70 $cm^{-1}$ in oscilloscope mode (integration time 0.15 s). Then laser power was set to 18 mW, and spectra were acquired (averaged from 3 repeats for each spot).

### 2.5. Spectral data analysis

Acquired SERS spectra were subjected to preprocessing which consisted of the following steps: 1) cropping to 400–1800 $cm^{-1}$ region; 2) baseline correction; 3) spike removal; 4) subtraction of Tris; 5) vector normalization. Then, for statistical classification PCA-LDA approach was utilized: first, Principal Component Analysis (PCA) was used to reduce dimensions of the data and keep only essential parts of it; then, Linear Discriminant Analysis (LDA) was applied to data with reduced dimensions (i.e. to PCs - principal components) for classification. Linear discriminants (LDs) were defined in a way that most efficiently separates two or more groups of objects. In particular, four viruses – CDV, MYXV, TMV, and PVX - were separated from each other. The Tris/control group was excluded from statistical classification due to irrelevance.

To estimate how well the results of the analysis would work on an independent data set, the classification models were validated. First, the Leave-One-Out (LOO) Cross Validation (CV) technique was used and then its accuracy was confirmed by repeated k-fold CV (5 repeats, 3 folds). It is noteworthy that instead of calculating PCs only once using all data PCs were re-calculated for each iteration using only train data subset, which increased the reliability of the validation.

For a better understanding of the results, LD coefficients were considered. Although in PCA-LDA each LD is a linear combination of PCs (not spectrum values), it is possible to express an LD in terms of spectrum values by multiplication of two matrixes: PCA loadings and LDA coefficients. Coefficients of such linear combination (LD in terms of spectrum values) are called LD coefficients in this work.

Spectra preprocessing steps 1–3 were carried out with OPUS 7.0 (Bruker) software. The remaining part of data analysis was performed with the R software [52]. In particular, following packages for R were used: hyperSpec [53] for data manipulations, base (*prcomp* function) [52] for PCA, MASS [54] for LDA, and caret [55] for CV; 3D scatter plot were performed by plotly [56] package for R, all other visualizations were created by ggplot2 [57] package.

For baseline correction, a standard concave rubber band method was used, with 64 points and 4 iterations. Muon-caused spikes were detected by visual inspection and then removed by straight-line generation. Tris spectrum was subtracted in two steps: (i) all spectra were normalized to the major peak of Tris (760–770 $cm^{-1}$); (ii) average spectrum of Tris/control group was subtracted from all spectra. Re-calculating of principal components within validation was implemented by '*preProcess*' parameter of caret's *train* function.

## 3. Results and discussion

### 3.1. SERS substrate properties and structure

The preparation of rough surfaces with nanocavities of specified size and spacing was maintained by adjusting the temperature of the mica substrate and accelerating voltage of the system. Depending on the temperature, voltage and the time of exposure, different types of surfaces could be fabricated, ranging from columnar microstructure with intercolumnar porosity to continuous rough terrain with semi-regularly spaced pore-like cavities.

The average size of apertures for manufactured novel substrates was in the range of 200–300 nm as determined with Gwyddion software from AFM and SEM data (Fig. 1). It provides a valuable tool for SERS measurements of particles with different diameters.

To develop a better understanding of the observed nanostructures, a comparison to structure zone models, developed for PVD processes by Movchan and Demchisin [58] and Thornton [59,60], is helpful. These models, enhanced with experimental results from various works on EBPVD and sputtering techniques, can be used to describe the influence of the substrate temperature on surface structure. The forming silver nanostructures exhibit patterns, predicted for zone I traits, existing under conditions of relatively low adatom mobility, with diffusion lifetime low enough to achieve surface roughness, but sufficiently high to avoid the formation of separate grains with distinct intercrystalline boundaries. The preferential growth of favored crystallographic directions leads to surface roughness, which, in turn, overshadows further growth of slower growing orientations. It results in the formation of metal "islands" that grow into columns or nanorods, and eventually merge and form one continuous surface with pore-like cavities. Lower temperature, shorter exposure, and higher deposition speed lead to more pronounced and discrete structures, while higher temperature, longer exposure and lower speed of deposition lead to smoother, less developed terrain.

In the present study, it was decided to obtain SERS spectra of several viral species to test the potential of the novel SERS substrates for virus detection. The temperature of mica substrate was set to 400 °C. The speed of deposition was 1–4 $Å s^{-1}$, with EB-acceleration voltage 9–11 kV and time of exposure approximately 90 min.

The average diameter of nanocavities in the substrate used in present study was 293 ± 51 nm, which corresponded to the diameter of animal viruses (200–300 nm for MYXV and 115–200 nm for CDV), intended for this study. This particular size was chosen because the majority of viruses should fit in, allowing a wider range of possible targets for the application of the novel SERS substrate. The average depth of the pore-like cavities was 11 ± 3 nm, the total volume of the pores was 8.8 $\mu m^3$, average pore quantity ~3 per $\mu m^2$. Cavities constituted up to 17% of the entire surface area of the substrate. Most important for nanoplasmonic properties of the substrate, however, are geometric parameters of the surface terrain. Root-Mean-Square Roughness Rq was 11.5 nm, 10-point average roughness Rz was 23.7 nm, calculated without counting the deepest parts of the pores (the darkest spots on Fig. 1). Kurtosis coefficient Rku was 11.6, which is much higher than normal distribution or values for columnar surfaces. Rku depicts the sharpness of the terrain, indicating the presence of rough edges and sharp turns within and near the pores.

Furthermore, the substrate was analyzed with X-ray Photoelectron Spectroscopy (XPS). The panoramic spectrum (Fig. 2a) contains mostly silver peaks, with additional signals, correlated with oxygen, carbon and minuscule amounts of copper. On Ag3d high-resolution spectrum (Fig. 2b) the tested SERS-substrate is compared with pure metallic silver. Both spectra are very similar, with the spectrum of the SERS-substrate having a slightly bigger arm at higher energies, indicating a bigger contribution from oxidized forms of silver. Com-

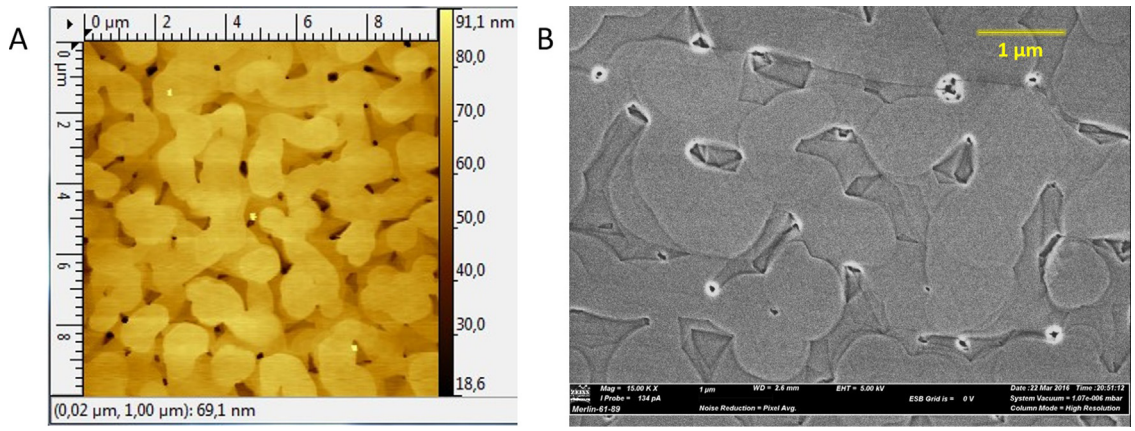


**Fig. 1.** Novel Ag nanofilm structure, demonstrated by AFM (A) and SEM (B) methods.

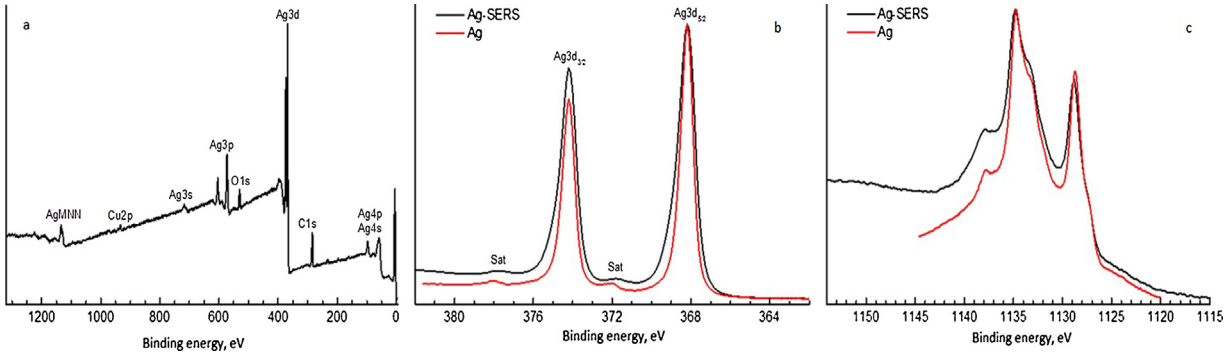


**Fig. 2.** a) Panoramic XPS spectrum of Ag SERS-substrate. b) Ag3d XPS spectra of pure silver [62] and SERS substrate. c) Ag NMM Auger spectra of pure silver [62] and SERS substrate.

**Table 1**
Comparison of XPS binding energies, kinetic energies of Auger electrons and Auger parameters for pure metallic silver and SERS substrate fabricated with the EBPVD method [62,63].

| | Silver SERS-substrate | Pure silver [62,63] |
|---|---|---|
| $E_{bind}(Ag3d_{5/2})$ | 368.2 eV | 368.21 eV; 368.3 eV |
| $E_{kinetic}(AgM_4NN)$ | 357.9 eV | 357.88 eV; 357.7 eV |
| Auger parameter | 726.1 | 726.09; 726.0 |

parison of the AgNMM Auger spectra (Fig. 2c) also demonstrates the similarity between SERS substrates and pure metal, which, for silver, is especially significant [61]. Generally, the energy of bonds, kinetic energy of Auger peaks and Auger parameter are almost identical to pure metallic silver (Table 1).

In conclusion, silver at the surface of the substrate remained mostly metallic, with only a small portion being oxidized. The carbon signals were also low, which indicated a minimal presence of surface contaminants. It coincides well with the general trend of better oxidation and erosion resistance of surfaces, coated by EBPVD methods.

### 3.2. SERS activity

It is known, that pores and pits contribution to surface enhancement is dependent on their diameter, with decreased SERS activity at pore sized bigger than 80 nm [64]. Smaller nanopores yield stronger SERS enhancements because of more pronounced curvatures and shorter interligament distance, which promote a bigger increase in localized electromagnetic fields. For pores/cavities larger than 100 nm in diameter, the major contribution to the electromagnetic enhancement must be due to the sharpness of the terrain, for instance, at the edges of the pore-like structures. High Rku values support this notion, indicating the presence of rapid drops and elevations at the surface.

The presence of SERS effect was observed by acquiring the spectra of different substances, including several proteins, thiocholine, Rhodamine-6G, Dithionitrobenzoic acid, glucose. On Fig. 3 the spectrum of glucose on the novel SERS substrate is compared against the spectrum taken from the same sample deposited on a non-enhancing smooth aluminum surface. Glucose does not covalently bind to silver and is not known for its strong SERS spectrum, which means that sufficient non-specific SERS-enhancement is achieved.

### 3.3. SERS spectra of viruses

The Ag substrates described above were applied to the detection of purified infectious agents. Initial studies were meant to determine whether the substrate could be used to collect SERS spectra of viruses and if so, to study the possibility to differentiate between different species based on their spectral properties. Vaccine strains of MYXV (strain IS-14) and CDV (strain "Ondeersteport"), as well as wild types of plant viruses – TMV (strain U1) and PVX (the Russian strain), were studied on the SERS substrate. Unique spectra were collected, with very distinct SERS signatures. All four viruses have different morphologies, with characteristic sizes allowing them to at least partially fit in the 300 nm wide nanoscale pores.

The concentration of viruses was set to $1 \times 10^9$ particles per ml. Considering the volume of virus sample (3 µl), the sample area covered by the dried sample on the SERS substrate (~7 000 000 $\mu m^2$), the virus concentration and the area of the sample spot probed during measurement, i.e. the laser spot size (~2.5 $\mu m^2$), this corre-

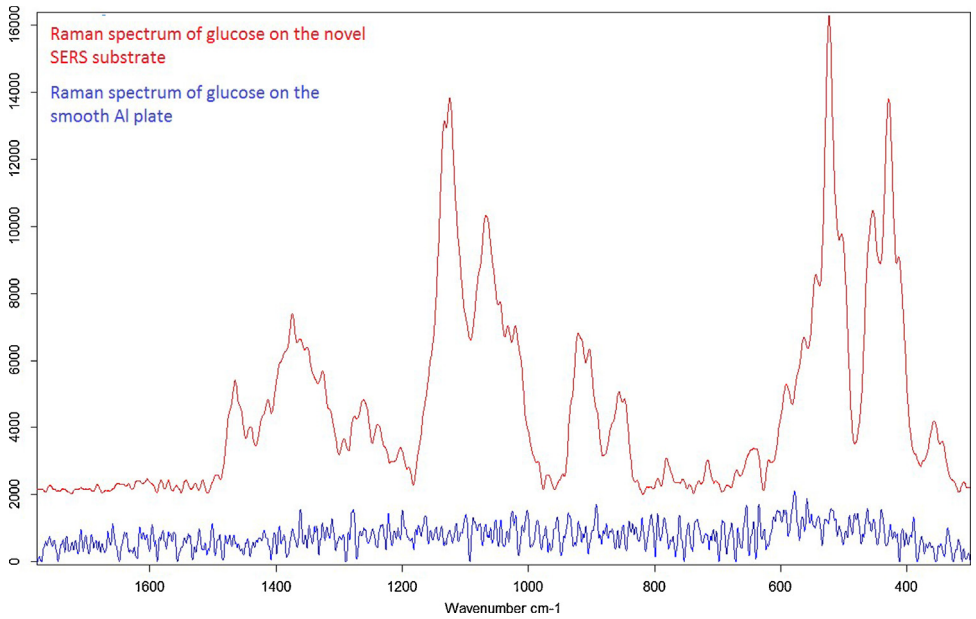


**Fig. 3.** Comparison of the Raman spectra of sample solution (glucose 0.01 g/l) on the novel Ag SERS substrate (red) and smooth Al substrate (blue), differences in integration time compensated by spectra multiplication. (For interpretation of the references to colour in this figure legend, the reader is referred to the web version of this article.)

sponds to the detection of about 1 viral particle per measurement area. Because the majority of particles are not infectious, it can be translated into a range of 0.01–0.2 PFU, depending on exact species and conditions. The calculated virion to nanopore ratio was 0.13, meaning that for every viral particle there were no less than 7.5 pores in the measurement area. Of course, Raman signals do not necessarily originate from intact viruses, but also from the components of damaged virions. Also, uneven distribution of analytes in the sample area is possible. In this study, the goal was to achieve unique and reproducible spectra, and sample concentration was set to achieve intense and easy to measure signals, which means that limits of sensitivity were not tested.

The optimal laser power was found to be 18 mW. The final dataset consisted of 137 SERS spectra (Fig. 4): 42 for Tris/control, 23 for CDV, 31 for MYXV, 10 for PVX, 31 for TMV. Except the PVX, spectra in all groups were acquired from several different batches of viruses at different dates, which introduced certain sample heterogeneity. Tris/control category consisted of 11 spectra from pure Tris solution, and 31 spectra from samples, obtained from uninfected *Vero* cells and plant material. These spectra were identical, which indicated that the purification process was effective. Due to redundancy, they were put into one group.

A Raman band assignment was performed by comparing the SERS spectra with typical Raman assignments of bulk virus material and single assemblies from the literature [65–68] and are given in Table 2. All SERS bands can be attributed to standard shifts of biochemical entities. The SERS-active surfaces interact predominantly with surface proteins, resulting in typical protein Raman bands in the measured SERS spectra. Due to the range of the evanescent field (<10 nm), in the SERS spectra of plant viruses (TMV and PVX), the Raman bands of the RNA could be seen in the SERS spectra as well. All four viruses have differences in their SERS spectra intensity and band position. Assignments were performed over the Raman shift range from 400 to 1800 $cm^{-1}$, which contains the majority of information. As illustrated (Fig. 5), this spectral region is most significant since it contains features representative of Raman-active compounds present in viral particles.

It can be seen, that viral spectra were dominated by features, corresponding to protein and nucleic acid content, as well as lipids and fatty acids, present in animal viruses. Although it is problematic to unambiguously identify specific molecules responsible for any particular shifts, they are likely related to species-specific epitopes present on the virus particle surface. Since SERS is primarily an interfacial analysis technique, it can be utilized to investigate only surficial compounds and immediate underlying parts ( <10 nm in depth). Comparison between two animal and two plant viruses revealed some expected key differences, such as peaks present in MYXV and CDV spectra, corresponding to cholesterol and other lipid content, as well as β-sheets typical for membrane proteins (610, 1067-69, 1098, 1302, 1443, 1448, 1491, 1676, 1734 $cm^{-1}$), and lack thereof in the spectra of TMV and PVX (Table 2). It is also noteworthy, that shifts typical for nucleic acids, while present in all spectra, were much more pronounced in the TMV and PVX spectra. It could be explained by their thin structure, which allows for signal enhancement of the innermost parts of the virus.

To confirm the possibility of reliable differentiation between species, all spectra were subjected to multivariate data analysis. The spectra were categorized into four groups - CDV, MYXV, TMV, and PVX. Then the PCA-LDA approach was used for classification of the four sample types based solely on their intrinsic spectra. The classification model was calculated and then validated. The LOO-CV technique was used, and it showed 100% accuracy. To ensure that it was not a false assessment, accuracy of the model was double checked by 5 times repeated 3-fold CV. It showed an average of 99,4% accuracy. Projection to LDs demonstrated a solid difference between groups (Fig. 6).

To determine the parts of spectral data that contribute most to the difference between groups, a correlation between average spectra and corresponding LD coefficients was tested (Fig. 7). As a first approximation, the high value of a coefficient indicates a higher intensity for a corresponding group (sample) at that band compared to other groups. Respectively, lower value means lower intensity. Although it is not standard LDA approach, such interpretation provides comprehensive information on parts of spectra that allow discrimination. For example, LD2 separated PVX from other species: the higher LD2 values were at approximately 470 $cm^{-1}$, 820 $cm^{-1}$, 850–870 $cm^{-1}$, 1050 $cm^{-1}$, 1500 $cm^{-1}$ and could be correlated to higher intensities at corresponding shifts in contrast to

**Table 2**
Raman shifts of peaks on the spectra of tested viruses and their possible band assignment.

| Raman shift ($cm^{-1}$) | | | | Possible band assignment |
|---|---|---|---|---|
| CDV | MYXV | TMV | PVX | |
| 420 | 421 | – | 421 | Adenine, Histidine [65], Cholesterol [66] |
| 449 | | | | Tryptophan [65], phenyl group [67] |
| 455 | 457 | 453 | 455 | Proline [65] |
| 468 | 468 | 466 | ~466 | Phenylalanine [65] |
| – | 493 | 493 | 493 | Guanine, Arginine, Tyrosine, D-(C)-Mannose (in gl. proteins) [65] |
| 505 | – | – | – | Glycine, Tryptophan [65] |
| – | 525 | – | – | Proline [65], S-S disulfide stretching in proteins, Phosphatidylserine, n(S-S) ν(S-S) ggt cysteine [67] |
| 532 | – | – | – | Alanine, Adenine [65] |
| – | – | 542 | 540 | Valine, Histidine [65], n(S-S) tgt cysteine, Glucose-saccharide (in gl. proteins) [67], |
| 551 | 551 | 552 | 552 | Arginine [65] |
| 565 | 569 | 569 | 569 | Guanine, Cytosine, Xylose (in gl. proteins) [65] |
| – | – | – | 594 | Tryptophan [65] |
| 599 | | | | Cytosine, Tryptophan [65], nucleotide conformation [67] |
| 610 | 610 | – | – | Serine, Arginine [65], Cholesterol [66] |
| – | 622 | – | – | Adenine, Phenylalanine, Histidine, D-(C)-Mannose (in gl. Proteins) [65], phenylalanine [67] |
| 627 | – | 626 | 626 | Tryptophan, [65] |
| 648 | 647 | 648 | 648 | Guanine [65], Tyrosine [67] |
| – | 664 | 666 | 666 | Valine [65], G, T (DNA/RNA) [67] |
| – | 676 | – | 679 | G (DNA), C [67] |
| 685 | – | 685 | ~685 | Glycine, Tryptophan, D-(C)-Mannose (in gl. proteins) [65] |
| 704 | 703 | – | – | Cholesterol, cholesterol ester [66] |
| – | – | 706 | 707 | L-Tryptophan [65], ν(C-S) t methionine [67] |
| – | – | 722 | – | Adenine [65] |
| – | 728 | – | 728 | C—C stretching, proline, adenine [67] |
| 732 | – | – | – | Histidine [65], Phosphatidylserine [66] |
| ~746 | ~746 | 746 | – | Phenylalanine, Proline [65], T (DNA/RNA), tryptophan [67] |
| – | ~762 | 762 | 761 | Tryptophan, δ(ring) [67] |
| – | – | – | 780 | Tryptophan [65], Uracil, C/U ring breathing (nucleotide) [67] |
| ~784 | 784 | 786 | – | Histidine [65], Phosphodiester, cytosine, U, T, C (DNA/RNA), O-P-O (DNA), cytosine, uracil, thymine, Pyrimidine [67] |
| 793 | – | – | – | Cytosine, Glutamate, Proline [65] |
| 809 | – | – | – | Glutamate [65], Phosphodiester (Z-marker) [67] |
| – | 826 | 825 | 824 | Valine, Histidine [65], O-P-O stretch DNA, Phosphodiester [67] |
| 834 | – | – | – | Phenylalanine, Proline [65] |
| 858 | 855 | 856 | 858 | Serine, Glutamate [65], Proline, hydroxyproline, tyrosine [67] |
| 881 | – | 879 | ~880 | Hydroxyproline, Tryptophan, ρ(CH 2) (proteins) [67] |
| – | 884 | – | – | Proteins [67] |
| 911 | – | – | 908 | Glucose (in gl. proteins) [67] |
| ~929 | ~929 | ~929 | 929 | Histidine [65], ν(C-C) in proline and valine (proteins) [67] |
| 939 | – | 936 | – | Guanine [65], Proline, C—C backbone, ν(C—C) residues (α-helix), C—O—C glycosides [67] |
| 961 | 958 | – | – | Phosphate [67] |
| 977 | – | 974 | ~974 | Histidine [65],Ribose (RNA) [67] |
| – | – | ~981 | 981 | Thymine, Uracil, Arginine [65], C—C stretching β-sheet (proteins) [67] |
| 1007 | 1006 | 1008 | 1007 | Phenylalanine, Tryptophan, Serine [65,67] |
| 1033 | 1034 | 1035 | ~1035 | Valine, Proline [65], Phenylalanine [65,67] |
| – | – | – | 1057 | Glutamate [65] |
| 1067 | 1069 | – | – | Arginine [65], Proline [67], Triglycerides, fatty acids [65–67] |
| 1098 | 1098 | – | – | Glutamate, fatty acids [65], Phosphodioxy ($PO_2^-$) groups, lipids [66,67] |
| – | – | 1104 | 1108 | Cytosine, Valine, Tryptophan [65], Phenylalanine [67] |
| 1130 | 1132 | 1131 | – | Saccharides [67] |
| 1147 | – | – | – | Alanine, Valine, glucose (in gl. proteins) [65] |
| 1162 | – | 1161 | 1160 | Adenine, Glutamate, Tryptophan [65], C—C/C—N stretching (proteins) [67] |
| 1175 | 1175 | – | – | Tyrosine, Phenylalanine [65,67], Cytosine, Guanine [67] |
| – | – | 1178 | – | Valine, tyrosine [65], Cytosine, Guanine [67] |
| 1209 | 1210 | 1211 | 1211 | ν(C—$C_6H_5$), Tryptophan [65,67], Phenylalanine, Tyrosine, Amide III [67] |
| 1235 | – | – | – | Guanine, Uracil, Alanine [65], Amide III [67] |
| 1259 | 1257 | – | – | Glycerol, fatty acids, glutamate [65], Adenine, Guanine and Cytosine, Amide III [67] |
| – | – | 1254 | 1255 | Uracil, tryptophan [65] |
| – | – | 1265 | 1267 | Guanine, tyrosine, proline [65], Amide III (α-helix) [67] |
| 1279 | ~1279 | 1279 | ~1279 | Tryptophan [65], Amide III (α-helix) [67] |
| 1302 | ~1302 | – | – | Triglycerides (fatty acids), lipids [67,68], Amide III [67] |
| 1323 | 1323 | ~1320 | 1320 | G (DNA/RNA), Amide III (α-helix) [67] |
| 1344 | 1343 | 1343 | 1342 | G (DNA/RNA), $CH_3$, $CH_2$ wagging, Glucose, δ(CH) residual vibrations [67] |
| 1364 | – | – | – | Tryptophan, Guanine [67] |
| 1391 | 1394 | 1394 | 1394 | Guanine, Uracil [65,67] |
| 1399 | – | – | – | Glycine, Valine [65] |
| 1420 | ~1420 | – | ~1420 | Glutamate [65], Deoxyribose (DNA), A,G (DNA/RNA) [67] |
| – | – | 1426 | – | Valine, serine [67] |
| – | 1443 | – | – | Triglycerides (fatty acids), Cholesterol [67] |
| 1448 | ~1448 | – | – | Lipids, proteins [66,67] |
| – | – | 1452 | ~1452 | Proteins [67] |
| 1466 | ~1466 | ~1463 | 1463 | Adenine, Guanine, Alanine, Valine, Serine [65] |
| ~1485 | ~1485 | – | – | Tryptophan [65], G, A, purine base, Amide II [67] |
| 1491 | ~1491 | – | – | Cytosine, Thymine, fatty acids [65] |
| 1513 | 1512 | – | – | A, Cytosine [67] |

Table 2 (*Continued*)

| Raman shift ($cm^{-1}$) | | | | Possible band assignment |
|---|---|---|---|---|
| CDV | MYXV | TMV | PVX | |
| 1538 | 1538 | – | – | Glutamate, Histidine [65], Amide carbonyl group vibrations and aromatic hydrogens [67] |
| 1552 | ~1552 | – | 1555 | Histidine [65], Tryptophan, Amide II [67] |
| – | – | 1561 | – | Tryptophan [67] |
| 1579 | ~1579 | 1580 | – | Pyrimidine ring, Phenylalanine [67] |
| – | – | – | 1587 | Phenylalanine, hydroxyproline [67] |
| 1606 | 1607 | – | 1609 | Tyrosine, phenylalanine, Cytosine ($NH_2$) [67] |
| – | – | 1612 | – | Adenine, Serine [65], Tyrosine, Cytosine ($NH_2$) [67] |
| 1618 | 1617 | – | – | Tryptophan [65,67], Phenylalanine, Tyrosine [67] |
| 1643 | – | – | – | Amide I (α-helix) [67] |
| – | 1659 | 1659 | 1658 | Cholesterol, Amide I (α-helix) [67] |
| 1662 | – | – | – | Valine [65], Nucleic acid [67] |
| 1676 | ~1676 | – | – | Fatty acids [65], Amide I (β-sheet), Cholesterol [66,67] |
| 1711 | – | – | – | Uracil, Arginine [65] |
| 1734 | 1734 | – | – | Esters, C&9552;O stretching (lipids) [67] |

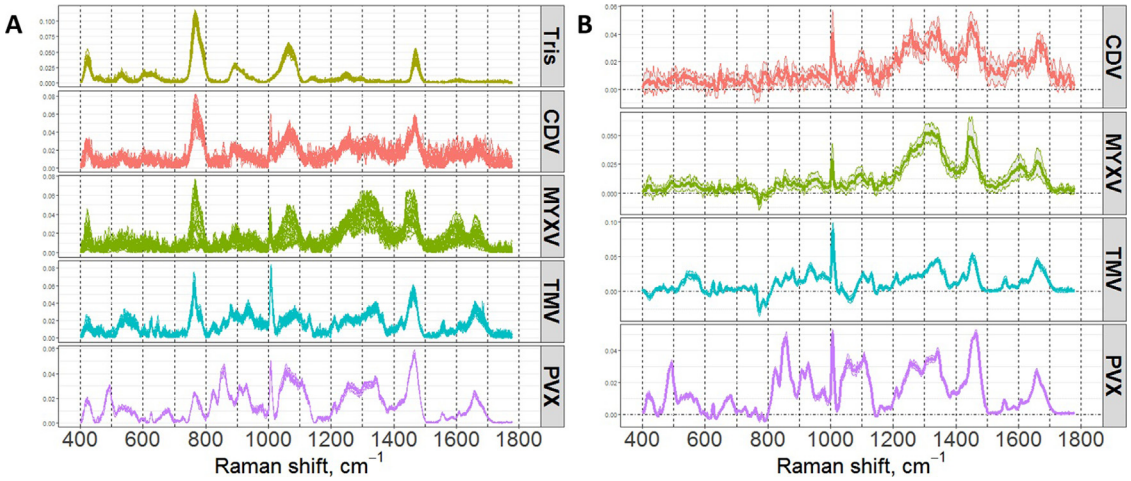


**Fig. 4.** A) Preprocessed (without subtracting tris/control) SERS spectra of (from top to bottom): Tris/control, CDV, MYXV, TMV, and PVX. B) Average ± standard deviation of preprocessed SERS spectra of viruses (used in PCA-LDA, tris/control subtracted).

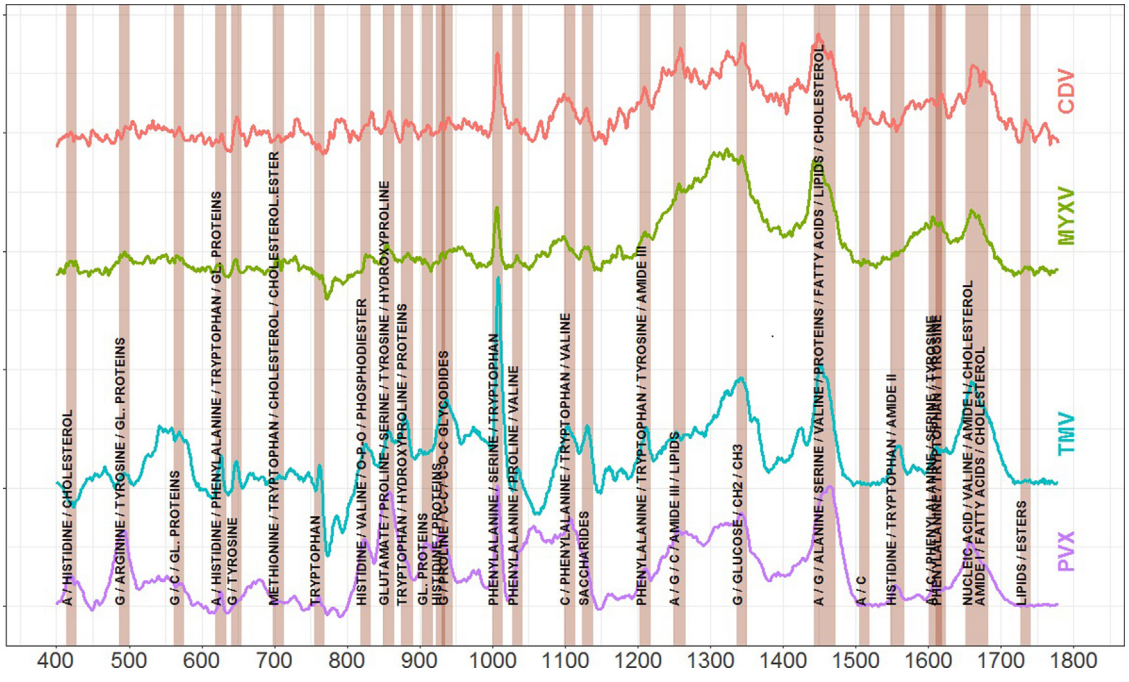


**Fig. 5.** Mean SERS spectra of CDV, MYXV, TMV, PVX, with labels, indicating some of the known Raman shift positions for common chemical groups.

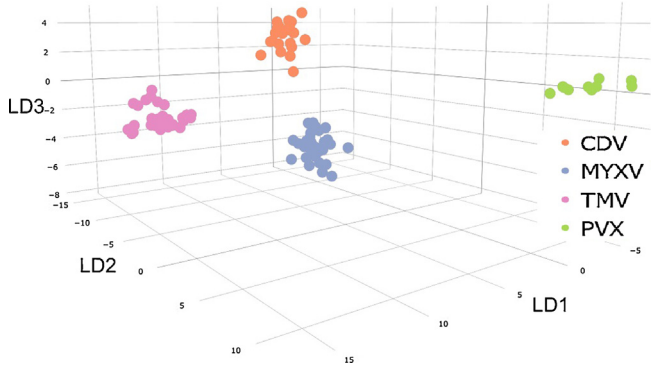


**Fig. 6.** Projections of the spectral data on the linear discriminants (LDs).

the spectra of other viruses. Likewise, the spectra of other viruses also had certain bands contributing to their distinctiveness, which could be indicated by higher positive or lower negative LD coefficients.

Some bands have high influence in all groups: 770–800 $cm^{-1}$, 1006–1008 $cm^{-1}$, 1430–1450 $cm^{-1}$, 1650–1700 $cm^{-1}$. These bands correspond to protein and RNA content, aromatic amino acids (especially Phenylalanine), lipid content, amide I peaks and more lipids, respectively. It coincides with described differences in peaks (Table 2) and reflects the dissimilarity in proteins (MYXV and CDV have larger variety of proteins), nucleic acids (TMV and PVX have stronger Raman signals from nucleic acids, MYXV has dsDNA, other species have RNA) and lipid content (MYXV and CDV are enveloped and have bilipid membranes, TMV and PVX are not enveloped). The bands that have high influence only in non-enveloped TMV and PVX, for example, ~480 $cm^{-1}$, ~850 $cm^{-1}$, 1560 $cm^{-1}$, mostly correspond to differences in amino acid composition.

Thereby, the classification of the spectra was accurate, which was evident in both peak parsing and multivariate data analysis. It proves that data classification was based on actual physical and chemical properties of the analyzed samples, which also testifies to the reliability of the novel SERS substrates in the Raman signal enhancement for biological substances.

## 4. Conclusions

Since the capabilities of SERS have reached the single molecule detection level, the largest limitation to SERS that remains unresolved is the requirement for target molecules and particles to be closely attached to SERS substrates. For large objects, such as viruses, it proves to be especially important to guarantee a tight interaction with the SERS-active surface. This issue was addressed with the development of a novel, cheap and easy to apply the technique for fabrication of porous SERS substrates with a rough surface, based on the EBPVD method. Compared with many of the existing techniques for SERS substrate fabrication, the EBPVD method offers several key advantages for nanofabrication, namely the combination of sufficient enhancements, high throughput, ease of preparation, reproducibility. The new SERS substrates have also been evaluated as potential bioanalytical sensors for virus detection. It was demonstrated that these substrates allow guaranteed differentiation between virus species and deep analysis of the spectral properties of the studied material. Data analysis showed that differences in spectra were not random, but corresponded to differences in chemical composition of viral particles. Therefore, the novel SERS substrates are applicable for biosensing.

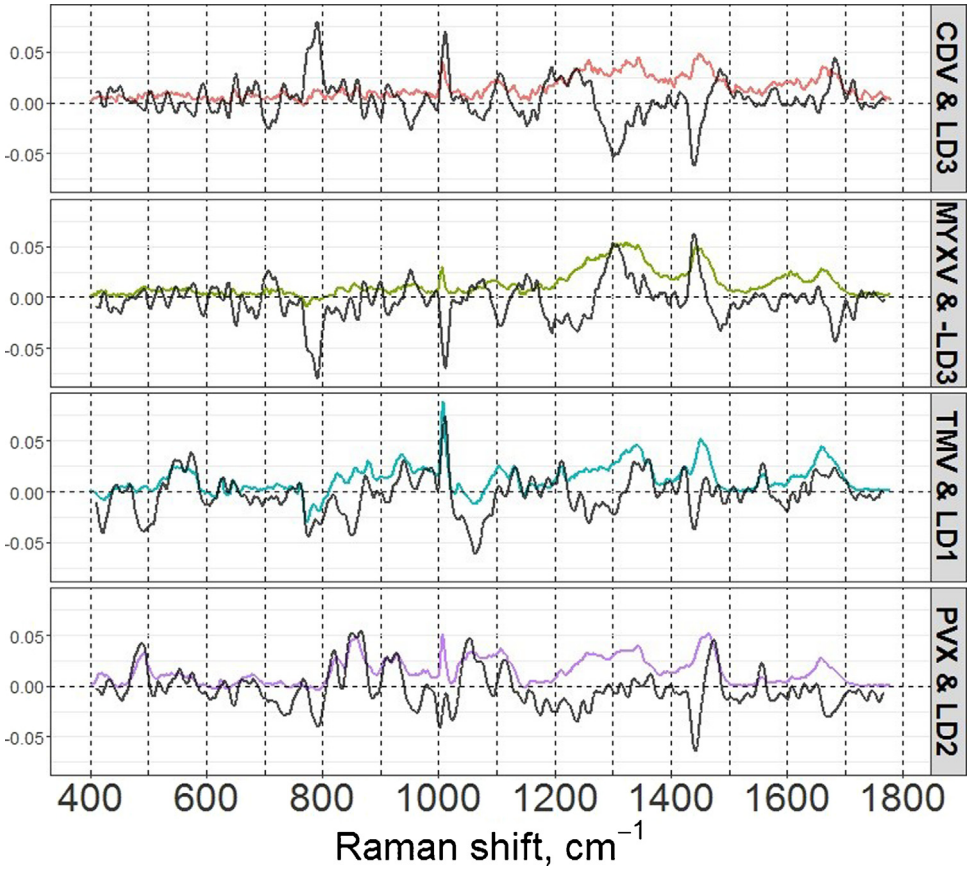


**Fig. 7.** Average SERS spectra of viruses (colored) with coefficients of corresponding LD (black). From top to bottom: CDV and coefficients of LD3, MYXV and inverted coefficients of LD3, TMV and coefficients of LD1, PVX and coefficients of LD2.

## Acknowledgements

SERS substrates were made at the BMSTU Nanofabrication Facility (Functional Micro/Nanosystems, FMNS REC, ID 74300). Facilities and equipment for the purification of viruses was provided by the A. N. Belozersky Institute of Physico-Chemical Biology, Lomonosov Moscow State University. The work was partially supported by Russian Science Foundation (RSF) (grant 16-14-00209).

## References

[1] H. Sharma, R. Mutharasan, Review of biosensors for foodborne pathogens and toxins, Sens. Actuators B 183 (2013) 535–549.
[2] S. Prasad, Nanobiosensors: the future for diagnosis of disease? Nanobiosens. Dis. Diagn. 3 (2014) 1–10.
[3] R.L. Atmar, Immunological Detection and Characterization, Springer, US, Birmingham, 2014, pp. 47–62.
[4] R.H. Sedlak, K.R. Jerome, Viral diagnostics in the era of digital PCR, Diagn. Microbiol. Infect. Dis. 75 (2013) 1–4.
[5] N. Boonham, J. Kreuze, S. Winter, R. van der Vlugt, J. Bergervoet, J. Tomlinson, R. Mumford, Methods in virus diagnostics: from ELISA to next generation sequencing, Virus Res. 186 (2014) 20–31.
[6] J. Jeong, H. Ju, J. Noh, A review of detection methods for the plant viruses, Res. Plant Dis. 20 (2014) 173–181.
[7] L.-A. Jaykus, Challenges to Developing Real-Time Methods to Detect Pathogens in Foods, 69, ASM News, 2003, pp. 341–347.
[8] J. Wang, M.J. Morton, C.T. Elliott, N. Karoonuthaisiri, L. Segatori, S.L. Biswal, Rapid detection of pathogenic bacteria and screening of phage-derived peptides using microcantilevers, Anal. Chem. 86 (3) (2014) 1671–1678.
[9] C.R. Taitt, G.P. Anderson, F.S. Ligler, Evanescent wave fluorescence biosensors, Biosens. Bioelectron. 20 (12) (2005) 2470–2487.
[10] N.E. Kurland, Z. Drira, V.K. Yadavalli, Measurement of nanomechanical properties of biomolecules using atomic force microscopy, Micron 43 (2–3) (2012) 116–128.
[11] C.A. Lopez, G. Daaboul, R. Vedula, E. Özkumur, D.A. Bergstein, T.W. Geisbert, H.E. Fawcett, J.H. Connor, B.B. Goldberg, M.S. Ünlü, Label-free, multiplexed virus detection using spectral reflectance imaging, Biosens. Bioelectron. 26 (8) (2011) 3432–3437.
[12] A. Balogh, M. Pap, L. Markó, I. Koloszár, L.K. Csatáry, J. Szeberényi, A simple fluorescent labeling technique to study virus adsorption in Newcastle disease virus infected cells, Enzyme Microb. Technol. 49 (3) (2011) 255–259.
[13] C.Y. Chiu, Viral pathogen discovery, Curr. Opin. Microbiol. 16 (2013) 468–478.
[14] V.V. Makarov, A.V. Khromov, V.A. Gushchin, A.P. Tkachuk, Emergence of new infections in the 21st century and identification of pathogens using next generation sequencing, Bull. Russ. State Med. Univ. 01 (2017) 5–25.
[15] M.I. Stockman, Nanoplasmonics: the physics behind the applications, Phys. Today 64 (2) (2011) 39–44.
[16] E.M. Larsson, S. Syrenova, C. Langhammer, Nanoplasmonic sensing for nanomaterials science, Nanophoton 1 (3-4) (2012) 249–266.
[17] A.-I. Henry, B. Sharma, M.F. Cardinal, D. Kurouski, R.P. Van Duyne, Surface-enhanced raman spectroscopy biosensing: in vivo diagnostics and multimodal imaging, Anal. Chem. 88 (13) (2016) 6638–6647.
[18] J.L. Abell, J.D. Driskell, R.A. Tripp, Y. Zhaod, Current progress on surface-Enhanced raman scattering Chemical/Biological sensing Func. Nanopart. Bioanal. Nanomed., and Bioelectron. Devices, 2, 2012, pp. 235–272.
[19] M. Prochazka, SERS investigations of cells, viruses and microorganisms, in: M. Prochazka (Ed.), Surface-Enhanced Raman Spectroscopy, Springer Int. Pub., Prague, 2015, pp. 127–146.
[20] P.P. Patra, R. Chikkaraddy, R.P.N. Tripathi, A. Dasgupta, G.V. Pavan Kumar, Plasmofluidic single-molecule surface-enhanced Raman scattering from dynamic assembly of plasmonic nanoparticles, Nat. Commun. (2014), http://dx.doi.org/10.1038/ncomms5357.
[21] T.A. Alexander, Development of methodology based on commercialized SERS-active substrates for rapid discrimination of poxviridae virions, Anal. Chem. 80 (2008) 2817–2825.
[22] M. Prochazka, Basics of surface-Enhanced raman spectroscopy (SERS), in: M. Prochazka (Ed.), Surface-Enhanced Raman Spectroscopy, Springer Int. Pub., Prague, 2015, pp. 1–59.
[23] P.L. Stiles, J.A. Dieringer, N.C. Shah, R.P. Van Duyne, Surface-enhanced raman spectroscopy, Annu. Rev. Anal. Chem. 1 (2008) 601–628.
[24] G.C. Schatz, M.A. Young, R.P. Van Duyne, Electromagnetic mechanism of SERS, in: K. Kneipp, M. Moskovits, H. Kneipp (Eds.), Surface-Enhanced Raman Scattering Physics and Applications, Springer, Berlin, 2006, pp. 19–46.
[25] C. Lee, C.S. Robertson, A.H. Nguyen, M. Kahraman, S. Wachsmann-Hogiu, Thickness of a metallic film, in addition to its roughness, plays a significant role in SERS activity, Sci. Rep. 5 (2015), http://dx.doi.org/10.1038/srep11644.
[26] M. Fan, G.F.S. Andrade, A.G. Brolo, A review on the fabrication of substrates for surface enhanced Raman spectroscopy and their applications in analytical chemistry, Anal. Chim. Acta 693 (2011) 7–25.
[27] S.-C. Luo, K. Sivashanmugan, J.-D. Liao, C.-K. Yao, H.-C. Peng, Nanofabricated SERS-active substrates for single molecule to virus detections in vitro: a review, Biosens. Bioelectron. 61 (2014) 232–240.
[28] C.-W. Chang, J.-D. Liao, A.-L. Shiau, C.-K. Yao, Non-labeled virus detection using inverted triangular Au nano-cavities arrayed as SERS-active substrate, Sens. Actuators B 156 (2011) 471–478.
[29] A.A. Stacy, R.P. Van Duyne, Surface enhanced raman and resonance raman spectroscopy in a non-aqueous electrochemical environment: tris(2,2'-bipyridine)ruthenium(II) absorbed on silver from acetonitrile, Chem. Phys. Lett. 102 (1983) 365–370.
[30] X. Zhang, Q. Zhou, Y. Huang, Z. Li, Z. Zhang, The nanofabrication application of substrates for surface-enhanced raman scattering, Int. J. Spectrosc. (2012), http://dx.doi.org/10.1155/2012/350684.
[31] N.A. Abu Hatab, J.M. Oran, M.J. Sepaniak, Surface-enhanced raman spectroscopy substrates created via electron beam lithography and nanotransfer printing, ACS Nano 2 (2) (2008) 377–385.
[32] N.D. Israelsen, C. Hanson, E. Vargis, Nanoparticle properties and synthesis effects on surface-enhanced raman scattering enhancement factor: an introduction, Sci. World J. (2015), http://dx.doi.org/10.1155/2015/124582.
[33] I.N. Kurochkin, I.A. Ryzhikov, A.K. Sarychev, K.N. Afanasiev, I.A. Budashov, M.V. Sedova, I.A. Boginskaya, S.V. Amitonov, E.V. Korostilev, A.N. Lagarkov, Enhancement of SERS signal using new material based on cerium dioxide facet dielectric films, Moscow Univ. Chem. Bull. 70 (2015) 102–107.
[34] A.N. Lagarkov, I.A. Budashov, V. Chistyaev, A. Ezhov, A. Fedyanin, A. Ivanov, I.N. Kurochkin, S. Kosolobov, A. Latyshev, D. Nasimov, I.A. Ryzhikov, M. Shcherbakov, A. Vaskin, A.K. Sarychev, SERS-active dielectric metamaterials based on periodic nanostructures, Opt. Express 24 (7) (2016) 7133–7150.
[35] Y. Yan, J. Zhang, P. Xu, P. Miao, Fabrication of arrayed triangular micro-cavities for SERS substrates using the force modulated indention process, RSC Adv. 7 (2017) 11969–11978.
[36] R.M. Stöckle, V. Deckert, C. Fokas, R. Zenobi, Controlled formation of isolated silver islands for surface-Enhanced raman scattering, Appl. Spectrosc. 54 (2000) 1577–1583.
[37] Z.-X. Yan, Y.-L. Zhang, W. Wang, X.-Y. Fu, H.-B. Jiang, Y.-Q. Liu, P. Verma, S. Kawata, H.-B. Sun, Superhydrophobic SERS substrates based on silver-coated reduced graphene oxide gratings prepared by two-beam laser interference, ACS Appl. Mater. Interfaces 7 (2015) 27059–27065.
[38] H.O. Chu, S. Song, C. Li, D. Gibson, Surface enhanced raman scattering substrates made by oblique angle deposition: methods and applications, Coat 7 (2) (2017), http://dx.doi.org/10.3390/coatings7020026.
[39] K. Bobzin, E. Lugscheider, R. Nickel, Modeling and simulation in the production process control and material property calculation of complex structured EB-PVD TBCs, Comput. Mater. Sci. 39 (3) (2007) 600–610.
[40] A.S. Baburin, A.R. Gabidullin, A.V. Zverev, I.A. Rodionov, I.A. Ryzhikov, U.V. Panfilov, Silver films deposited by electron-beam evaporation for application in nanoplasmonics. herald of the bauman Moscow state tech. univ, Instrum. Eng. 6 (2016) 4–14.
[41] P.J. Kerr, J. Liu, I. Cattadori, E. Ghedin, A.F. Read, E.C. Holmes, Myxoma virus and the leporipoxviruses an evolutionary paradigm, Viruses 7 (3) (2015) 1020–1061.
[42] B. Sawatsky, S. Delpeut, V. von Messling, Canine distemper virus, in: S.K. Samal (Ed.), The Biology of Paramyxoviruses, Caister Academic Press, Norfolk, 2011, pp. 275–291.
[43] K. Namba, G. Stubbs, Structure of tobacco mosaic virus at 3.6 A resolution: implications for assembly, Science 231 (1986) 1401–1406.
[44] C. Lico, E. Benvenuto, S. Baschieri, The two-faced potato virus X: from plant pathogen to smart nanoparticle, Front. Plant Sci. (2015), http://dx.doi.org/10.3389/fpls.2015.01009.
[45] D. Whitehouse, Surfaces and Their Measurement Butterworth-Heinemann, Warwick, 2004.
[46] S.E. Smallwood, M.M. Rahman, D.W. Smith, G. McFadden, Myxoma virus: propagation, purification, quantification, and storage, Curr. Protoc. Microbiol. 14A (1) (2010), http://dx.doi.org/10.1002/9780471729259.mc14a01s17.
[47] A.M. Armitage, H.J. Cornwell, N.G. Wright, A.R. Weir, Determination of the buoyant density of canine distemper virus by radioassay, Arch. Virol. 47 (1975) 319–329.
[48] K.C. Stallcup, S.L. Wechsler, B.N. Fields, Purification of measles virus and characterization of subviral components, J. Virol. 30 (1) (1979) 166–176.
[49] M.D. Duarte, S.C. Barros, A.M. Henriques, M.T. Fagulha, F. Ramos, T. Luís, M. Fevereiro, Development and validation of a real time PCR for the detection of myxoma virus based on the diploid gene M000.5L/R, J. Virol. Methods 196 (2014) 219–224.
[50] E.A. Trifonova, N.A. Nikitin, M.P. Kirpichnikov, O.V. Karpova, J.G. Atabekov Obtaining, Characterization of spherical particles—new biogenic platforms, Moscow Univ. Biol. Sci. Bull. 70 (2015) 194–197.
[51] N. Nikitin, A. Ksenofontov, E.A. Trifonova, M. Arkhipenko, E. Petrova, O. Kondakova, M.P. Kirpichnikov, J.G. Atabekov, E. Dobrov, O.V. Karpova, Thermal conversion of filamentous potato virus X into spherical particles with different properties from virions, FEBS Lett. 590 (2016) 1543–1551.
[52] R Core Team, R: A Language and Environment for Statistical Computing, R Foundation for Statistical Computing, Vienna, Austria, 2016 https://www.R-project.org/.
[53] C. Beleites, V. Sergo, 'hyperSpec: a package to handle hypersectral data sets in R&#39 R package version 0 98-20150304. http://hyperspec.r-forge.r-project.org/.
[54] W.N. Venables, B.D. Ripley, Modern Applied Statistics with S, fourth edition, Springer, New York, 2002.
[55] M. Kuhn, caret: Classification and Regression Training. R Package Version 6, 2016, pp. 0–71 https://CRAN.R-project.org/package=caret.

[56] C. Sievert, C. Parmer, T. Hocking, S. Chamberlain, K. Ram, M. Corvellec, P. Despouy, plotly: Create Interactive Web Graphics via 'plotly.js'. R Package Version 4.5.6, 2016 https://CRAN.R-project.org/package=plotly.
[57] H. Wickham, ggplot2: Elegant Graphics for Data Analysis, Springer-Verlag, New York, 2009.
[58] B.A. Movchan, A.V. Demchishin, Study of the structure and properties of thick vacuum condensates of nickel titanium, tungsten, aluminium oxide and zirconium dioxide, Phys. Met. Metallogr. 28 (1969) 83–90.
[59] J.A. Thornton, Influence of apparatus geometry and deposition conditions on the structure and topography of thick sputtered coatings, J. Vac. Sci. Technol. A 11 (1974) 666–670.
[60] J.A. Thornton, High rate thick films, An. Rev. Mat. Sci. 7 (1977) 239–260.
[61] V.K. Kaushik, XPS core level spectra and Auger parameters for some silver compounds, J. Electron. Spectrosc. Relat. Phenom. 56 (1991) 273–277.
[62] J.F. Moulder, W.F. Stickle, P.E. Sobol, K.D. Bomben, Handbook of X-ray Photoelectron Spectroscopy, ULVAC-PHI, Inc., Chigasaki, 1995, p 261.
[63] M.P. Seah, Reference data for Auger electron spectroscopy and X-ray photoelectron spectroscopy combined, App. Surf. Sci. 144–145 (144) (1999) 161–167.
[64] A. Kassu, C. Farley, A. Sharma, W. Kim, J. Guo, Effect of pore size and film thickness on gold-coated nanoporous anodic aluminum oxide substrates for surface-enhanced raman scattering sensor, Sensor 15 (2015) 29924–29937.
[65] J. De Gelder, K. De Gussem, P. Vandenabeele, L. Moens, Reference database of Raman spectra of biological molecules, J. Raman Spectrosc. 38 (2007) 1133–1147.
[66] C. Krafft, L. Neudert, T. Simat, R. Salzer, Near infrared Raman spectra of human brain lipids, Spectrochim. Acta A 61 (2005) 1529–1535.
[67] Z. Movasaghi, S. Rehman, I.U. Rehman, Raman spectroscopy of biological tissues, Appl. Spectrosc. Rev. 42 (2007) 493–541.
[68] E. Katainen, M. Elomaa, U.-M. Laakkonen, E. Sippola, P. Niemelä, J. Suhonen, K. Järvinen, Qualification of the amphetamine content in seized street samples by Raman spectroscopy, J. Forensic Sci. 52 (2007) 88–92.

## Biographies

**N.N. Durmanov** received his MS degree in Biochemistry from Lomonosov Moscow State University, Russia in 2013. After working in Gamalei Science Research Center of Epidemiology and Microbiology until 2015, he became a junior researcher in Emanuel Institute of Biochemical Physics of Russian Academy of Sciences. His main research interests are biosensors for medical and environmental applications.

**R.R. Guliev** was born in Moscow, Russia in 1990. He received his MS degree in Applyed mathematics and informatics from Lomonosov Moscow State University, Russia in 2013. From 2013 till 2016 he received postgraduate education at Emanuel Institute of Biochemical Physics, Russian Academy of Sciences, Moscow, Russia. Now he is a junior researcher at the same institute. His main research interests revolve around multivariate data analisys, spectral data analysis in particular.

**A.V. Eremenko** received his MS degree in Pharmaceutical Chemistry from 1-st Moscow Medical Institute, Russia in 1982. In 1986 he obtained his Ph.D. in Biochemistry and Pharmacology from Institute of Pharmacology, Russian Acad. Medical Sci. Moscow. Now he is leading researcher in Emanuel Institute of Biochemical Physics of Russian Academy of Sciences. His main research interests are biosensors for medical and environmental applications.

**A. Boginskaya** received her MS degree in Materials of Micro-, Opto- and Nanoelectronics from Moscow State University of Fine Chemical Technologies in 2009. In 2012 she obtained Ph.D. in Technology and Recycling of Polymers and Composites and in Powder Metallurgy and Composite Materials. Currently she is working as a researcher in the Institute for theoretical and applied electromagnetics of Russian Academy of Sciences in the laboratory of Nanotechnology of composite materials and thin film structures.

**A. Ryzhikov** received his MS degree in Technical Physics from Moscow Engineering Physics Institute in 1977. In 2000 he obtained his Ph.D. in Electrophysics in Institute for theoretical and applied electromagnetics Russian Academy of Sciences. Now he is the head of the laboratory of Nanotechnology of composite materials and thin film structures in the same institute.

**E. A. Trifonova** received her MS degree in Biochemistry from Lomonosov Moscow State University, Russia in 2010. In 2013 she obtained Ph.D. in Virology from Lomonosov Moscow State University, Russia. Currently she works as a senior research at the Department of Virology of the Lomonosov Moscow State University.

**E.V. Putlyaev** recieved his MS degree in Virology from Lomonosov Moscow State University, Russia in 2011. In 2015 he obtained his Ph.D. in Virology from Lomonosov Moscow State University, Russia. Currently he works as a fellow scientist at the Virology department of the biology faculty of the Lomonosov Moscow State University, Russia.

**A.N. Mukhin** received his MS degree in Biochemistry from Moscow State Academy of Veterinary Medecine and Biotechnology - MVA by K.I. Skrybin, Russia in 1997. In 2000 he obtained his Ph.D. in Virology from The All-Russian State Center for Quality and Standardization of Veterinary Drugs and Feed (VGNKI), Russia. At present he is a Senior Researcher in the Laboratory of Virus Deseases of Diagnostics and Prevention Research Institute and Senior Research Scientist in the laboratory of Virus Diseases Specific Prevention, Institute of Virology of N.F. Gamaleya Federal Research Centre for Epidemiology and Microbiology, Ministry of Health, Moscow, Russia.

**S.L. Kalnov** received his MS degree in Biochemistry from Lomonosov Moscow State University, Russia in 1975. In 1980 he obtained his Ph.D. in Biochemistry from Lomonosov Moscow State University, Russia. At present he is Head of Laboratory of Diagnostics and Prevention Research Institute and Senior Research Scientist in the laboratory of Virus Diseases Specific Prevention, Institute of Virology of N.F. Gamaleya Federal Research Centre for Epidemiology and Microbiology, Ministry of Health, Moscow, Russia.

**M.V. Balandina** received her MS degree in Veterinary Medicine from Scryabin Moscow State Academy of Veterinary Medicine and Biotechnology, Russia in 2001. In 2006 she obtained her Ph.D. in epizootology, virology and microbiology from Institute of Experimental Veterinary, Moscow, Russia. At present she is Head of Immunochemistry group and Senior Research Scientist in the laboratory of Molecular Diagnostics, Institute of Virology, N.F. Gamaleya Federal Research Centre for Epidemiology and Microbiology, Ministry of Health, Moscow, Russia.

**A.P. Tkachuk** received his MS degree in Molecular Biology from Lomonosov Moscow State University in 2007. He obtained his Ph.D. degree in Molecular Genetic from The Institute of Gene Biology Russian Academy of Science (Moscow, Russia) in 2010. Currently he works as a Head of the Translational biomedicine laboratory of the N.F. Gamaleya Federal Research Centre for Epidemiology and Microbiology. His current research activity deals with development of new methods of infectious disease detection, prophylactic and cure.

**A. Gushchin** was born in Chu, Kazakhstan, in 1987. He studied at the Russian State Agrarian University (Moscow, Russia) and Wageningen University from 2004 to 2009. He received the MS degree in Genetics in 2009 and the PhD degree in Molecular Biology, in 2015 at the Moscow State University (Moscow, Russia). Currently he works as a senior research fellow at the translational biomedicine laboratory of the N.F. Gamaleya Federal Research Centre for Epidemiology and Microbiology. His current research activity deals with development of new methods of infectious disease detection, prophylactic and cure.

**A.K. Sarychev** received his MS degree in Physics from Moscow Institute of Physics and Technology in 1974. He obtained his Ph.D. in Physics from Institute of High Temperatures, Russian Academy of Science, Moscow in 1978. In 1993 he obtained Doctor of Science degree in Applied Electrodynamics, Russian Academy of Science, Moscow. He is now a Principal scientist in the Institute for theoretical and applied electromagnetics of Russian Academy of Sciences. his main research directions are centered on Plasmonics of Nanostructured Materials.

**A.N. Lagarkov's** scientific career started in late 60 s in theretical department of the Joint Institute for High Temperatures, Soviet Academy of Science. He obtained his Ph.D. in 1967 and Doctor of Science degree in 1977 in Physical and Mathematical sciences. Since 1999 he is the director of the Institute for theoretical and applied electromagnetics, the then subdivision of the Joint Institute for High Temperatures, Russian Academy of Science, which became an independent institute in 2007.

**A. Rodionov** received his MSci degree in informatics and control systems from the Bauman Moscow State Technical University (BMSTU) in 2008. Subsequently in 2010 he received his Engineering Doctorate (Candidate of Science) in semiconductor technology from the BMSTU. From 2005 to 2013 he worked as a research Engineer in the lithography and photomask design group at the Scientific Research Institute of System Analysis of Russian Academy of Science (SRISA RAS), Moscow. Since 2013 he has been working as a head of research and educational center Fuctional Micro/Nanosystems (FMN) at BMSTU, Moscow. His research interests include the fabrication of plasmonic devices, nanophotonics and optics, lab-on-chip, photonics and MEMS sensors, quantum simulators and sensors.

**A.R. Gabidullin** received the BS degree in Electrical Engineering from the Bauman Moscow State Technical University (BMSTU) in 2015. Now he is working towards the M.S. degree in BMSTU. His research interests include the technology of thin films.

**N. Kurochkin** received his MS degree in Chemical Enzymology from Lomonosov Moscow State University, Russia in 1979. In 1985 he obtained his Ph.D. in Chemical Kinetics and Catalysis from Lomonosov Moscow State University, Russia. In 2003 he obtained Doctor of Science degree in Chemical Kinetic and Biotechnology at Lomonosov Moscow State University, Russia. Now he is Professor Chemical Department of Moscow State University and Director of Emanuel Institute of Biochemical Physics Russian Academy of Sciences.